Molecular Dynamics Study of Viscoelastic Properties of Confined Oligomer Melts

Asako Koike

Hitachi Research Laboratory, Hitachi Ltd., 7-1-1 Omika, Hitachi, Ibaraki 319-1292, Japan

Received September 11, 1997; Revised Manuscript Received March 9, 1998

ABSTRACT: The viscoelastic properties of oligomer melts (i.e., thin films) confined by two walls are studied from molecular dynamics simulations. The storage and loss moduli are calculated by shearing the upper wall periodically. The effects of film thickness, pressure, chain length, and wall−film interactions are investigated as a function of frequencies. Even if the film is thinner than 5 molecular diameters, frequency dependence of the basic viscoelastic properties follows Rouse theory. However, hardly any molecular-weight difference is seen in thin films in the high-frequency region. The loss modulus shows that viscosity decreases with increasing frequency as shown in surface force apparatus experiments. With higher pressure, the tendency becomes more noticeable and the nonlinear shear response increases and storage and loss moduli are almost the same, independent of frequency, like under the solid state. The storage and loss moduli calculated from the shear response by shearing the slider are also compared with those calculated by the Green−Kubo formula.

1. Introduction

The subjects of friction, wear, and adhesion are important for extending lifetime, getting greater reliability, and miniaturizing products. Thin liquid films are well-known for their ability to decrease friction and wear, and they have been widely used as lubricants for a long time. However, the mechanism of lubrication is not clearly understood. In recent years, using such precise apparatuses as an SFA (surface force apparatus)[1−5] and FFM (frictional force microscope)[6] and computer simulations[7−10], the behaviors of liquid thin films have been shown to differ from those of bulk. These results indicate that the thin liquid films confined by two walls are epitaxialized and crystallized with a low shear rate at temperatures higher than the glass transition temperature. These behaviors are sensitive to the film thickness and molecular structure and molecular weight.[1,2,7] The viscosity decreases with increasing shear rate.[3,4,10] Further, the kinetic friction of polymers is very unstable and easily changeable during repetitive shear.[5]

To get added insight into the dynamics of the liquid films, storage and loss moduli are good indices. This is because it is easy to distinguish between liquidlike and solidlike film by investigating the storage and loss moduli, and it is possible to measure the relaxation time of the molecules adsorbed onto the wall by investigating the frequency dependence of these moduli. For example, FFM showed the glass transition temperature of the surface of a film was lower than that of bulk.[11,12] The liquidlike-to-solidlike transition was also found to depend on the film thickness and molecular structure on the basis of the SFA.[9,13−15] However, experiments are not enough to understand what is the cause of these phenomena; rather a combination of computer simulations and experiments is useful. A look at the literature shows that storage and loss moduli of thin films have been investigated by hardly any computer simulations.

In this study, to get fundamental properties of storage and loss moduli of thin confined film, we examined the influence of the film thickness, pressure, and wall−film interactions. Further, by comparing the storage and loss moduli by shear simulation with those calculated by the Green−Kubo formula[16,17] in an equilibrium simulation, we investigated the extent of the large difference between the two methods and its cause.

2. Theory, Simulation Model, and Methods

2.1. Theory. It is widely recognized from the viewpoints of elasticity and hydrodynamics that the shear stress, which follows Hook's law, is directly proportional to the strain and the shear stress, which follows Newton's law of viscosity, is proportional to the rate of strain.[18] Accordingly, when one of the two walls which confine the film is moved periodically, the strain phase shifts from the shear stress phase. By separating the shear stress in the strain phase and in a 90°out-of-phase configuration, we can obtain a shear storage modulus G' and shear loss modulus G''.

Further, the following relations hold between spring constant k and G', and between viscosity η and G'',

$$G' = (h/S)k \tag{1}$$

$$G'' = \eta\omega \tag{2}$$

where h is the distance between two walls and S is the surface area of the walls.

On the other hand, viscoelasticity can also be calculated without shear by using the Green−Kubo (G−K) formula as follows.[16,17] The intrinsic viscosity can be written as

$$\eta^*(\omega) = \frac{V}{k_B T}\int_0^\infty \exp(-i\omega t)\, C(t)\, \mathrm{d}t \tag{3}$$

where V is the system volume and $C(t)$ is the correlation function of the stress tensor. One method to calculate the correlation function is as follows:[19]

$$C(t) = \frac{\langle \sum_{\alpha\beta} \delta P_{\alpha\alpha}(t)\, \delta P_{\beta\beta}(0)\rangle}{9} \tag{4}$$

$$\delta P_{\alpha\alpha}(t) = P_{\alpha\alpha}(t) - \langle P_{\alpha\alpha}\rangle \tag{5}$$

S0024-9297(97)01343-0 CCC: $15.00
Published on Web 06/18/1998

where the stress tensor $P_{\alpha\beta}$ is calculated by virial theory and $\alpha\beta$ = xy, yz, zx.

A newer, improved method has been shown by Mondello and Grest:[20]

$$C(t) = \frac{\langle \sum_{\alpha\beta} P_{\alpha\beta}(t)\, P_{\alpha\beta}(0) \rangle}{10} \tag{6}$$

$$P_{\alpha\beta} = (\sigma_{\alpha\beta} + \sigma_{\beta\alpha})/2 - \delta_{\alpha\beta}(\sum_{\gamma} \sigma_{\gamma\gamma}) \tag{7}$$

where the stress tensor $\sigma_{\alpha\beta}$ is calculated by virial theory.

The averaged correlation function of eqs 4 and 5 would be unstable within a possible simulation time in some cases. So we used the approach expressed by eqs 6 and 7. By separating the real and imaginary parts of the viscosity, the storage and loss moduli are calculated.

2.2. Simulation Model. Each system studied here was composed of a film confined by two walls with two-dimensional periodic boundary conditions in the plane of the walls. The films were composed of an oligomer with N6 (hexamers), N12 (dodecamers), N30 (tricontamers), and N60 (hexacontamers) segments per chain. The chains were modeled by using well-studied bead-spring chains.[21] The number of the segments composing each film was set as 1620. For comparison to thin film, the number of the segments was set as 3000. Hereafter, the previous film is referred to as thin film and the latter film as thick film. Each segment interacted with other segments with the distance r by purely repulsive, truncated, and short-ranged Lennard-Jones (LJ) potentials:

$$U(r) = 4\epsilon\left[\left(\frac{\sigma}{r}\right)^{12} - \left(\frac{\sigma}{r}\right)^{6} + \frac{1}{4}\right] \qquad r \le r_c \tag{8}$$

$$= 0 \qquad r > r_c$$

where ϵ is the LJ energy parameter and σ is the LJ length parameter. We used $\epsilon = 1.0$, $\sigma = 1.0$, and $r_c = 2^{1/6}\sigma$. The conductivity between adjacent segments of the same chain was kept by using strongly attractive finite extensible nonelastic spring potential:

$$U_{\text{bond}}(r) = -\frac{k}{2} R_0^{\,2} \ln\left[1 - \left(\frac{r}{R_0}\right)^2\right] \qquad r < R_0 \tag{9}$$

where r is the distance between adjacent segments, k is the energy parameter, and R_0 is a length parameter. We used $k = 30\epsilon\sigma^{-2}$ and $R_0 = 1.5\sigma$ to prevent chains from virtual crossing.[21]

Each wall was composed of a triple-layered (111) fcc surface with a lattice constant of 3.334σ and the number of segments composing each wall was 486. The area of the wall was $225\sigma^2$. The potential between a segment of the film and that of the wall was also modeled by eq 8 and $\epsilon_w = 1.5\epsilon$ was used. Two values of r_c were used, $2^{1/6}\sigma$ and 2.5σ. The former is referred to as the repulsive wall and the latter as the attractive wall. When not specified, reference is always to the repulsive wall. Stiff springs were employed for the wall segment to preserve the fcc lattice:[22]

$$U_{dw}(d) = \frac{1}{2} k_w d^2 \tag{10}$$

where d is the atomic deviation from the fcc lattice and k_w is the spring constant. If rigid wall were used, the frictional force would be almost the same as that of the flexible wall with springs. However, the rigid wall would easily slip over the film. Thus, we used $k_w = 72\epsilon/2^{1/3}\sigma$, which prevents wall melting.[22]

2.3. Simulation Methods. The initial coordinates of the films were generated by random number. To get a well-equilibrated configuration, we simulated at the normal load per area $10\epsilon/\sigma^3$ for 200τ ($\tau = (m\sigma^2/\epsilon)^{1/2}$; m is the monomer mass) at the temperature T, $kT = 15\epsilon$, 200τ at $kT = 10\epsilon$ with $10\epsilon/\sigma^3$, 200τ at $kT = 5\epsilon$ with $10\epsilon/\sigma^3$, and 200τ at $kT = \epsilon$ with $15\epsilon/\sigma^3$. When the normal load per area for the shear simulation was changed, the normal load per area was set as 10, 22.5, or $30\epsilon/\sigma^3$ in the final step at $kT = \epsilon$. When we used attractive walls, the equilibrated films, confined by repulsive walls, were used as initial coordinates and we equilibrated them for 500τ at a constant volume in order to compare the results at the same density with those of repulsive walls. Accordingly, the system condition is shown by densities in the attractive walls simulation and by pressures in the repulsive walls simulation.

The upper wall was sheared as $x(t) = A \sin(2\pi t/T)$, $T = 10\tau - 4000\tau$. The simulations were carried out for $1000\tau - 24000\tau$. The shear response was averaged for every cycle except the first one.

In the simulations to calculate the storage and loss moduli by the G−K formula, the slider height was fixed and the simulations were carried out for 15000τ.

The temperature was kept at $kT = \epsilon$ by using Berendsen's thermostat.[23] To remove the thermal energy caused by friction, the walls and film were controlled separately. When the upper wall was moved, the temperature was two-dimensionally controlled by y- and z-directions, since a priori, it would be broken in the shear direction (x-direction). The distance between the two walls was kept constant under shear. Newton's equation of motion was integrated by a leapfrog algorithm[24] with a time step of 0.005τ.

3. Results

3.1. Influence of Amplitude. When the shear strain is large, the viscoelastic behavior of the film contains a nonlinear term. When the shear response is nonlinear, the shear stress is expressed as follows.[25] The even order frequencies are canceled out because of symmetry of the shear strain, γ.

$$\sigma = \sum_{n=1,\text{odd}} (G'_n \gamma_0^n \sin n\omega t + G''_n \gamma_0^n \cos n\omega t) \tag{11}$$

Here, γ_0 is the strain amplitude and the following relation holds:

$$G_n^* = G'_n + iG''_n \tag{12}$$

To get some insight into the nonlinear shear response, we investigated the relation between oscillation amplitude and storage and loss moduli for N30 at pressure $15\epsilon/\sigma^3$ with the repulsive walls as shown in Figure 1. Figure 1 indicates that until the oscillation amplitude of 2.5σ is reached, storage and loss moduli are almost the same, independent of the amplitude. However, when the amplitude is larger than 2.5σ, they decrease. Since the spring constant is derived from the storage modulus in eq 1, Figure 1 indicates that the spring constant decreases with increasing amplitude. The

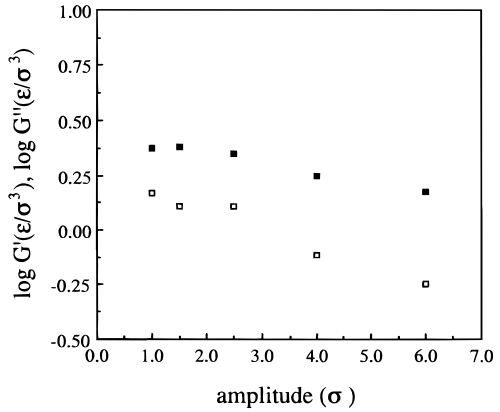

Figure 1. Amplitude dependence of the storage and loss moduli of N30 with density $0.76\sigma^{-3}$ and the film thickness is 6.8σ.

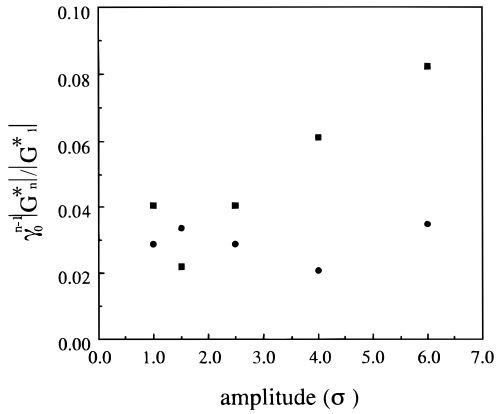

Figure 2. Amplitude dependence of higher-order harmonics normalized by $\gamma_0|G_1^*|$. Filled squares represent $\gamma_0^2|G_3^*|/|G_1^*|$ and filled circles represent $\gamma_0^4|G_5^*|/|G_1^*|$.

decrease of storage moduli has also been observed experimentally.[14] Figure 2 shows the amplitude dependence of higher-order harmonics, $\gamma_0^3|G_3^*|$ and $\gamma_0^5|G_5^*|$, normalized by $\gamma_0|G_1^*|$. With increasing amplitude, the largeness of $\gamma_0^2|G_3^*|/|G_1^*|$ increases, although $\gamma_0^4|G_5^*|/|G_1^*|$ does not change significantly. Details of the nonlinear response have been discussed by Matsumoto et al.,[25] and the work done by moving the upper wall is as follows:

$$W = \int_0^\tau \sigma\dot{\gamma}\, \mathrm{d}t \tag{13}$$

Here, the shear strain is represented by

$$\dot{\gamma} = \omega\, \gamma_0 \cos \omega t \tag{14}$$

By substituting eqs 11 and 14 into eq 13, the work concerning G_3^* and G_5^* is written as

$$W_{G_3'} = G_3'\gamma_0^4\left\{-\frac{\cos 4\omega t}{8} - \frac{\cos 2\omega t}{4} + \frac{3}{8}\right\} \tag{15}$$

$$W_{G_3''} = G_3''\gamma_0^4\left\{\frac{\sin 4\omega t}{8} + \frac{\sin 2\omega t}{4}\right\} \tag{16}$$

$$W_{G_5'} = G_5'\gamma_0^6\left\{-\frac{\cos 6\omega t}{12} - \frac{\cos 4\omega t}{8} + \frac{5}{24}\right\} \tag{17}$$

$$W_{G_5''} = G_5''\gamma_0^6\left\{\frac{\sin 6\omega t}{12} + \frac{\sin 4\omega t}{8}\right\} \tag{18}$$

Equations 15−18 indicate that the work concerning G_3^* and G_5^* is elastic work with periodicity π/ω or $\pi/2\omega$. Accordingly, the increase of the nonlinear response of G_3^* and G_5^* is not caused by relaxation releasing the strain energy but by the potential energy surface shape as a function of strain.

3.2. Comparison with Rouse Theory. In an undiluted state, according to Rouse theory, which neglects hydrodynamics interaction between segments, the storage and the loss moduli are expressed as follows:[18]

$$G' = (\rho RT/M)\sum_{p=1}^{N} \omega^2\tau_p{}^2/(1 + \omega^2\tau_p{}^2) \tag{19}$$

$$G'' = (\rho RT/M)\sum_{p=1}^{N} \omega\tau_p/(1 + \omega^2\tau_p{}^2) \tag{20}$$

where M is molecular weight and ρ is the density. In the range of $\omega \geq 1/\tau_e$ ($t > \tau_e$; the molecule feels the constraints imposed by tube), the frequency dependence of the storage and loss moduli can be expressed as follows:

$$G' = G'' = \sqrt{3}/2(\rho RT\eta_0/M)^{1/2}\omega^{1/2} \tag{21}$$

$$\eta_0 = (\rho RT/M)\tau_1 S_1 \tag{22}$$

where ρ is the density and S_1 is 1.645. That is, the slope of the storage and loss moduli curves are about 0.5 at high frequency. Further, according to Rouse theory, G' and G'' scarcely change in $1/\tau_d < \omega < 1/\tau_e$ (τ_d is the reptation time) and this region is called a plateau zone.[26] Here, $\tau_e < \tau_r$ (Rouse time) $< \tau_d$. The plateau zone and the zone in which the slope of the storage and loss moduli curves is about 0.5 have been found in experiments in the bulk state[18] and a confined thin film.[13]

To get some insight into the relaxation time of the film for which frequency dependence of storage and loss moduli was calculated, we estimated the Rouse time of the film confined by attractive walls (hereafter abbreviated as τ_r^{att}) from the longest relaxation time of the time correlation function of the end-to-end vector of the molecules. As a comparison, we also calculated Rouse time in the bulk state (τ_r^{bulk}) and with the repulsive wall (τ_r^{rep}) with same densities and same film thicknesses. It is also possible to estimate the Rouse (τ_c) time from viscosity which is the value before shear thinning as follows:[26]

$$\tau_c = \frac{12M\eta}{\pi^2\rho RT} \tag{23}$$

where η is the viscosity. These Rouse times, the radius of gyration R_g, and the anisotropy of R_g are summarized in Table 1. Table 1 shows that the difference between τ_r^{rep} and τ_r^{att} increase with increasing density. Bitsanis and Hadziioannou[27] showed that the difference in diffusion time of the molecules and the longest relaxation time of the molecules when confined by repulsive walls and by attractive walls is very small. This was because they used low densities around $0.65\sigma^{-3}$ and set a little small energy depth between a wall and the molecules. Table 1 also shows that τ_c is shorter than τ_r^{att}. It is also possible theoretically to calculate τ_e, τ_r,

Table 1. Pressure, Film Thickness, Density, R_g (Radius of Gyration), and the Anisotropy of R_g and Rouse Time of Each System[a]

molecule	pressure (ϵ/σ^3)	density ($1/\sigma^3$)	film thickness (σ)	R_g^{bulk} (σ)	R_g^{rep} (σ)	R_g^{att} (σ)	anisotropy of R_g^{att}	anisotropy of R_g^{rep}	τ_r^{bulk} (τ)	τ_r^{rep} (τ)	τ_r^{att} (τ)	τ_c (τ)
N12	2.0	0.74	11.5	1.72	1.69	1.69	1.17	1.15	45	45	130	79
											295	103
	4.0	0.89	9.5	1.67	1.68	1.66	1.17	1.15	90	130	(95)	(102)
			(18.9)									
	7.0	1.02	8.3	1.62	1.66	1.59	1.18	1.10	195	490	665	192
	15.0	1.25	6.8		1.55			1.19		≅30 000		
N30	2.0	0.75	11.3	2.95	2.95	2.79	1.26	1.26	450	550	650	386

[a] The pressure is that measured by repulsive walls with film. The anisotropy of $R_g = (R_g^x + R_g^y)/2R_g^z$, R_g^z is the R_g of the radius of gyration of the axis perpendicular to the walls. τ_r^{bulk}, τ_r^{rep}, and τ_r^{att} are the Rouse time of bulk, confined by repulsive walls and confined by attractive walls as estimated from the correlation function of the end-to-end vector. τ_r^{att},in parentheses, is that of thick film. τ_c is the Rouse time estimated from eq 23.

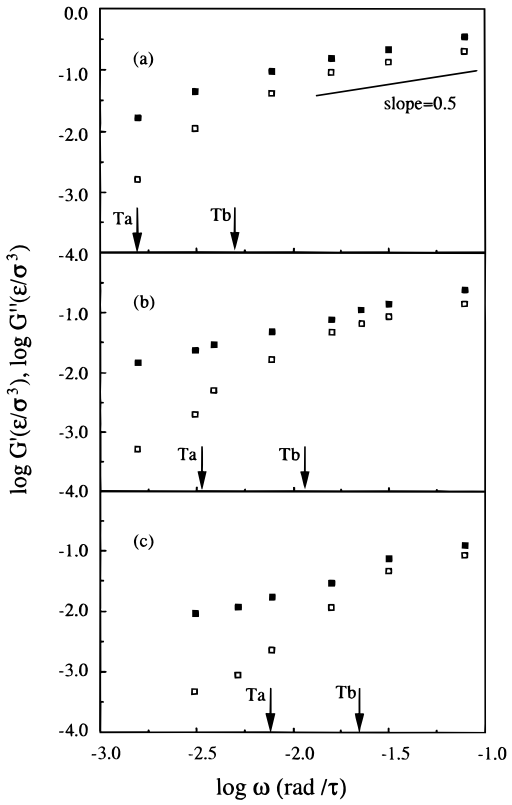

Figure 3. Frequency dependence of storage and loss moduli of N12 with densities of (a) 1.02, (b) 0.89, (c) $0.74\sigma^{-3}$. The film thicknesses are 8.3, 9.5, and 11.5 σ, respectively. T_a and T_b represent logarithms of the inverse of Rouse time of attractive walls and bulk, respectively. As a guide, the slope = 0.5 is shown in (a).

and τ_d from the mean-square displacement of the segments $g(t)$,[26] because $g(t)$ changes as follows: $g(t) \propto t^{1/2}$, $t < \tau_e$; $g(t) \propto t^{1/4}$, $\tau_e < t < \tau_r$; $g(t) \propto t^{1/2}$, $\tau_r < t < \tau_d$; $g(t) \propto t$, $t > \tau_d$. The results of these simulations show that $g(t)$ is roughly proportional to $t^{1/2}$ in all time scales and we cannot estimate the relaxation times. This was because the molecular length was too short compared to the critical entangled length N_e. Kremer and Grest[28] showed that τ_e in bulk was about 1800τ and N_e was 35 with density $\rho = 0.85\sigma^{-3}$ from $g(t)$ by using the same kind of bead-spring model. Accordingly, when N is smaller than 30 with $\rho \cong 0.85\sigma^{-3}$, τ_e is expected to be larger than τ_r. Even if τ_e is longer than τ_r due to a confinement effect of the film, the difference between τ_e and τ_r is expected to be small.

Figure 3 shows the frequency dependence of storage and loss moduli of N12 films with attractive walls for different low densities. The slope changes at a different time with different density and every slope is about 0.5 in the high-frequency region as expected by Rouse theory. Figure 3 also shows that Rouse time of the film becomes shorter with decreasing density and the critical frequency (ω_c), at which the slope of the storage and loss moduli becomes 0.5, becomes higher. Figure 3 indicates that ω_c is larger than $1/\tau_r^{att}$ and rather close to $1/\tau_r^{bulk}$ and $1/\tau_c$. Table 1 shows that τ_r^{att} is longer than τ_c. There are two possible reasons for the time difference between ω_c and $1/\tau_r^{att}$. One is the time difference between τ_r^{att} and τ_e. However, this can be eliminated from the viewpoint of critical entangled length as mentioned above. The other is that τ_r^{att} has a broader distribution than that of τ_r^{bulk}. Figure 4 shows τ_r^{att} as a function of distance from the walls. This figure shows that τ_r^{att} close to the walls is much longer than that inside the films. The time difference between the τ_r^{att} of regions close to the walls and that inside the films becomes larger with increasing densities. Further, τ_r^{att} inside the films is shorter than the averaged τ_r^{att} of the whole film in Table 1 and close to τ_c and close to $1/\omega_c$ in Figure 3.

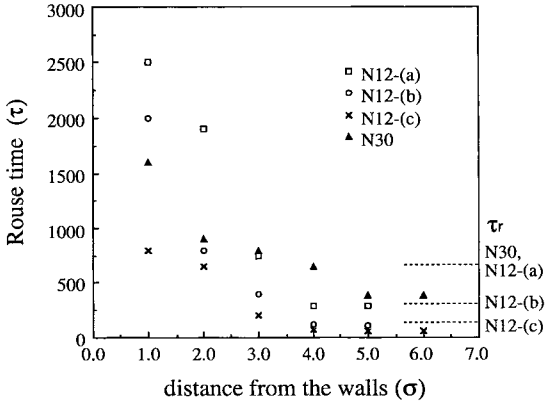

Figure 4. The Rouse time τ_r^{att} as a function of the distance from the walls. The densities of N12-(a), N12-(b), N12-(c), and N30 are 1.02, 0.89, 0.74, and $0.75\sigma^{-3}$, respectively. As a guide, the averaged Rouse times of the whole film τ_r^{att} are shown on the right side.

To get further insight into τ_r^{att} distribution, we also calculated the frequency dependence of storage and loss moduli of thick films as shown in Figure 5. τ_r^{att} of the thick film is close to that of the bulk as shown in Table 1. Figure 5 shows that critical frequency ω_c of thick film is a little higher than that of thin film. However, the critical frequency difference is much smaller than

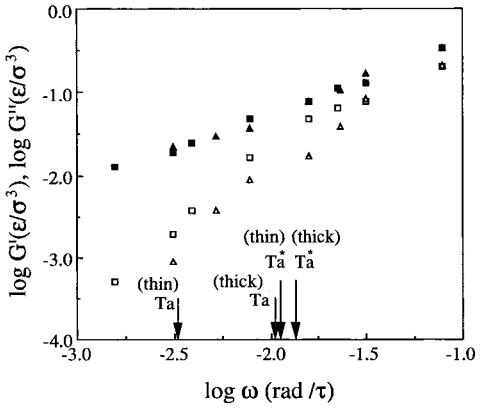

Figure 5. Comparison between thin (squares) and thick (triangles) film of N12 with density $0.89\sigma^{-3}$. The open symbols represent storage moduli and shaded symbols represent loss moduli. Film thickness are 9.5 and 18.9σ. T_a and T_a^* represent logarithms of the inverse of Rouse time τ_r^{att} of the whole film and inside the film, respectively.

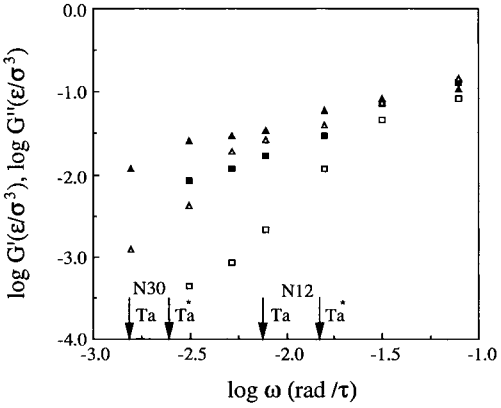

Figure 6. Comparison between storage and loss moduli of N12 (squares) and N30 (triangles). The open symbols represent storage moduli and shaded symbols represent loss moduli. Both films have a thickness of 9.5σ with densities of 0.74 (N12) and $0.75\sigma^{-3}$ (N30).

the difference between $1/\tau_r^{att}$ of whole film. τ_r^{att} inside the films are about 70τ (thin film) and 90τ (thick film), indicating that critical frequencies and the critical frequency difference are rather close to the $1/\tau_r^{att}$ inside the films and their difference. From these results, we can conclude that, in confined thin film, τ_r^{att} of the film becomes longer and ω_c becomes smaller than in bulk. However, since the influence of the wall is restricted in regions close to the wall, ω_c is higher than the estimated values from τ_r^{att} of the whole film and rather close to those from τ_r^{att} inside the film. Thus, the confined effect is smaller than that estimated from τ_r^{att} of the whole film.

To investigate the influence of the molecular length, we also calculated frequency dependence of storage and loss moduli of N30. This is shown in Figure 6. ω_c of N30 is lower than that of N12. Figure 6 also shows that ω_c is closer to $1/\tau_r^{att}$ inside the film and $1/\tau_c$ rather than $1/\tau_r^{att}$ of the whole film. In the SFA experiment for a confined thin film, the entangled effect (G' becomes larger than G'' in the plateau region) has been seen in comparatively small molecular-weight molecules which would not show clear entanglement effect in the bulk condition.[14] Figure 6 does not show a plateau region or entangled effect. Unfortunately, for $N > 30$ with

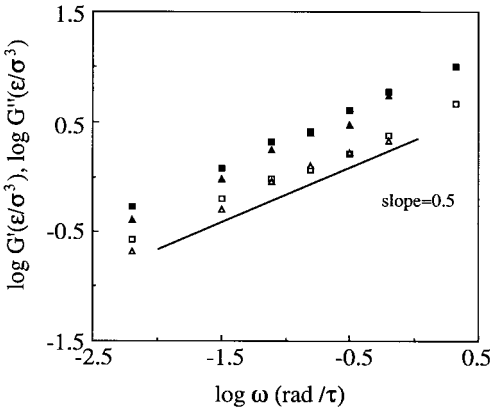

Figure 7. Comparison between storage and loss moduli of N12 confined by attractive walls (triangles) and by repulsive walls (squares). Both films have a thickness of 6.8σ with a density of $1.25\sigma^{-3}$. The open symbols represent storage moduli and shaded symbols represent loss moduli.

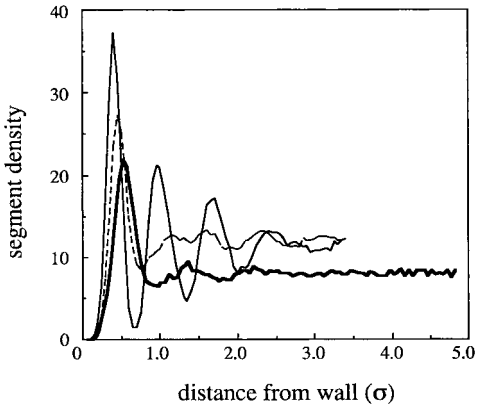

Figure 8. Segment density profiles as a function of a distance from the wall of N12 confined by attractive walls (solid line) and repulsive walls (dashed line) with density $1.25\sigma^{-3}$ and N12 confined by attractive walls (thick solid line) with density 0.89 σ^{-3}.

these densities, τ_r^{att} is too long to investigate the entangled effect and $\rho = 0.75\sigma^{-3}$ is the lowest density at which the storage and loss moduli can be measured accurately. Accordingly, we could not investigate the entanglement effect.

At these low densities, the film cannot follow the repulsive slider movement and we could not measure those density films with repulsive walls. However, at comparatively high densities, the film can follow the repulsive slider movement. Figure 7 shows the frequency dependence of storage and loss moduli of films confined by attractive and repulsive walls at high density. The slopes of storage and loss moduli of attractive and repulsive walls are 0.5 in all frequency regions which is much higher than $1/\tau_r$. It is interesting to note that both moduli of attractive walls are almost the same as those of repulsive walls. In both systems, the velocity gradient is uniform under shear and there are no slips. The segment densities of both systems and at low density with attractive walls are plotted in Figure 8. Figure 8 shows that the segments of attractive walls at high density are highly ordered parallel to the walls, though they are not ordered at low density. The attractive walls have an influence over the film structure, but not over the storage and loss moduli.

These results led us to the conclusion that the behaviors of a liquid film thinner than 5 diameters of the molecules are consistent with Rouse theory.

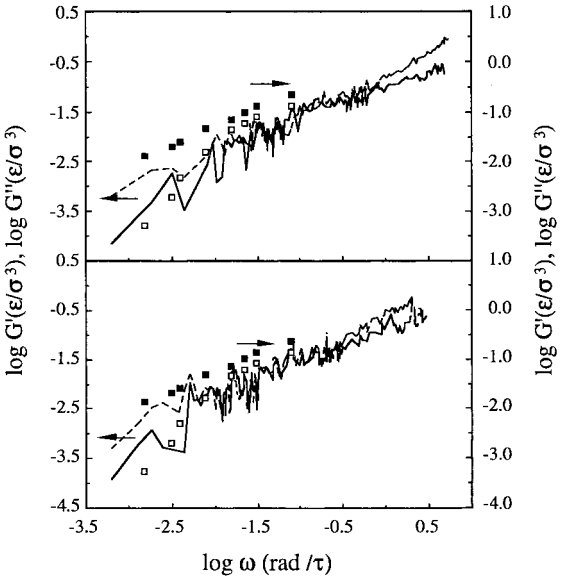

Figure 9. Comparison between storage and loss moduli of N12 calculated from the G−K formula and those from the shear response by shearing the upper wall. The film thickness is 9.5σ with density 0.89 σ^{-3}. Open and shaded squares represent storage and loss moduli calculated from the G−K formula, respectively. Solid and dotted lines represent storage and loss moduli calculated from the shear response by shearing the upper wall. (a) These are calculated from the *xy*-component in the G−K formula. (b) These are calculated from all off-diagonal components.

3.4. Viscoelasticity by the Green−Kubo Formula. Viscoelasticity is usually calculated by the G−K formula for a diluted solution.[17] It is also possible to calculate the viscoelasticity of an undiluted solution by the G−K formula as expressed in section 2.1. Within the range of nonlinear response, the storage and loss moduli calculated by the G−K formula will be consistent with those calculated from the shear response by moving the slider periodically. But, in a confined system, the symmetry of the system is broken. Accordingly, we calculated viscoelasticity by two kinds of stress tensors, one calculated from all off-diagonal components and the other calculated from only the *xy*-component. Figure 9a,b compares the storage and loss moduli calculated from the shear response for N12 with an amplitude of 2.5σ with attractive walls and those calculated from the G−K formula for the two kinds of stress tensors. There are almost no differences between Figure 9a and 9b. Figure 9a,b indicates that the frequency dependence of the storage and loss moduli of both calculation methods is roughly similar; however, moduli from the G−K formula are smaller than those from shear response. In the lower frequency range below critical frequency, the slope of the storage and loss moduli lines in Figure 9a,b are almost 0.5 and are consistent with the Rouse theory. Further, the critical frequency of G−K and those from shear response are almost the same. From eqs 21 and 22, the logarithm of the storage and loss moduli at log $\omega = 0.0$ is 0.18 and this value is close to that from the shear response. There is some possibility for unsuitability of the correlation function of the pressure tensor, because the number of atoms making up the film is too small. However, the difference at all frequencies in the two methods is expected to be too large, if the reason is error due to the small system size. Since Figure 2 shows that even for amplitudes of $1-2.5\sigma$, nonlinear shear response is observed slightly, we interpret the findings as follows. The linear shear response amplitude region is very narrow and when the amplitude is outside that region, the storage and loss moduli become larger because of the potential surface roughness of the film which is a function of a strain. However, it is difficult to calculate the storage and loss moduli at amplitudes smaller than 1σ, because the shear response becomes too small to calculate precisely. There is room for further investigation of this difference between the two methods.

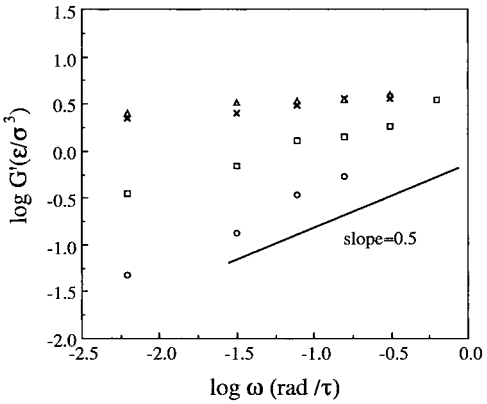

Figure 10. The frequency dependence of the storage moduli of N30 under different pressures. Circles, squares, x's and triangles represent pressures of 10, 15, 22.5, and $30\epsilon/\sigma^3$, respectively.

3.5. Effects of Pressure. Figure 10 shows frequency dependence of G' or G_1' of N30 with repulsive walls for different pressures (densities). R_g and anisotropy of R_g of the film which we used in this and the next sections are summarized in Table 2. Although R_g is almost the same, independent of pressure, the anisotropy of the R_g increases with increasing pressure. Rouse time is much longer than the periodic time T in these conditions. At higher pressures of 22.5 and $30\epsilon/\sigma^3$, nonlinear shear response has been observed in as small an amplitude as measurable. Accordingly, G_1' is plotted instead of G'. When the pressure is lower than $10\epsilon/\sigma^3$, the phase of shear stress of the upper wall and that of the base are a little different, since the velocity gradient within the film is not uniform. Accordingly, we could not measure storage and loss moduli at lower pressures than $10\epsilon/\sigma^3$. The slopes of storage moduli are about 0.5, in 10 and $15\epsilon/\sigma^3$, and consistent with Rouse theory in undiluted solution as mentioned in section 3.2. On the other hand, when pressures are 22.5 and $30\epsilon/\sigma^3$, there is almost no frequency dependence of the shear storage moduli. Concerning loss moduli, the slopes are also about 0.5 in 10 and 15 ϵ/σ^3 and there is almost no frequency dependence in 10 and $15\epsilon/\sigma^3$. Further, the storage moduli of 22.5 and $30\epsilon/\sigma^3$ are almost the same in Figure 10, and this indicates that these storage moduli are the maximum limit for the spring model. In the crystalline state and amorphous solid, storage and loss moduli are known to be slightly frequency dependent.[18] Accordingly, this indicates that the film in 22.5 and $30\epsilon/\sigma^3$ is of the solid state. The liquid−solid transition was experimentally observed in a confined film when there was a big decrease of the ratio G''/G'.[14] In our simulations, G''/G' in 22.5 and $30\epsilon/\sigma^3$ becomes smaller than those in 10 and $15\epsilon/\sigma^3$ but are still larger than 1. This is expected to be because the interaction between segments is only from the repulsive force.

Figure 11 shows the frequency dependence of $\gamma_0^3|G_3^*|$ and $\gamma_0^5|G_5^*|$ normalized by $\gamma_0|G_1^*|$ at pressures of 22.5

Table 2. Pressure, Density, Film Thickness, R_g, and Anisotropy of R_g and Rouse Time τ_r of Each System with Repulsive Walls[a]

molecule	pressure (ϵ/σ^3)	density ($1/\sigma^3$)	film thickness (σ)	R_g (σ)	anisotropy of R_g	τ_r (τ)
N6	15.0	1.24	6.8	1.23	1.21	≅20 000
			(12.9)	(1.10)	(1.06	
N12	15.0	1.25	6.8	1.55	1.19	≅30 000
			(12.8)	(1.57)	(1.09)	
N30	10.0	0.76	7.6	2.53	1.35	≅7000
	15.0	1.12	6.8	2.51	1.50	≅40 000
	22.5	1.25	6.3	2.61	1.63	
	30.0	1.35	6.0	2.56	1.70	
N60	15.0	1.41	6.9	4.17	2.25	
			(12.6)	(3.84)	(2.27)	

[a] Rouse times at high pressure are longer than the possible computational time. The film thickness, R_g, and anisotropy of R_g in parenthes are those of thick film.

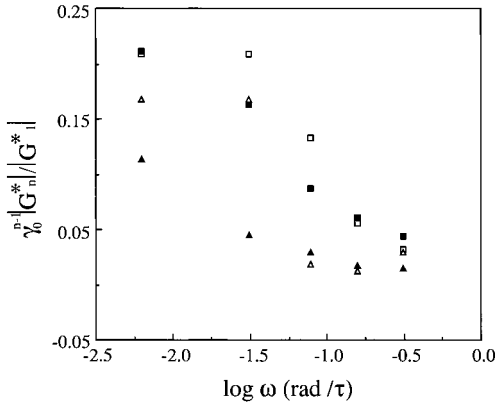

Figure 11. The frequency dependence of nonlinear responses of $\gamma_0^3|G_3^*|$ and $\gamma_0^5|G_5^*|$ normalized by $\gamma_0|G_1^*|$. Triangles represent those of pressure = $22.5\epsilon/\sigma^3$ and squares represent those of $30\epsilon/\sigma^3$. Open symbols represent $\gamma_0^2|G_3^*|/|G_1^*|$ and shaded symbols represent $\gamma_0^4|G_5^*|/|G_1^*|$.

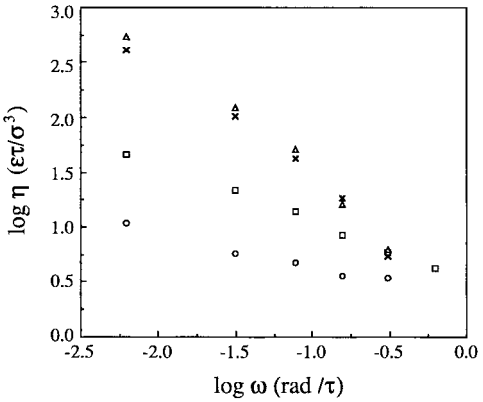

Figure 12. The frequency dependence of the viscosity of N30. Circles, squares, x's and triangles represent viscosity with pressures of 10, 15, 22.5, and $30\epsilon/\sigma^3$, respectively.

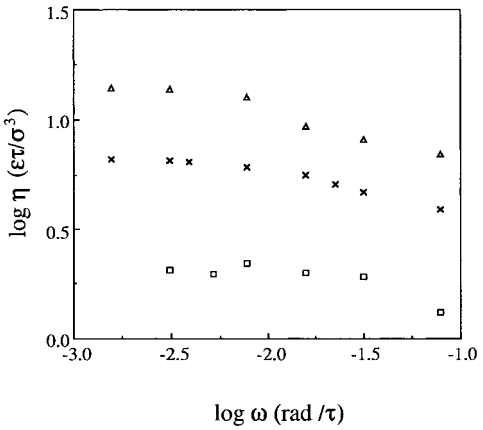

Figure 13. The frequency dependence of the viscosity of N12. Squares, x's, and triangles represent viscosity with densities of 1.02 (b) 0.89 (c) $0.74\sigma^{-3}$, respectively.

and $30\epsilon/\sigma^3$. $\gamma_0^2|G_3^*|/|G_1^*|$ and $\gamma_0^4|G_5^*|/|G_1^*|$ monotonically increase with frequency decrease at high pressure. Apparent slips between walls and the film or slips within the film are not observed in any system. We interpreted these non linear responses as follows. At high pressure, the intermolecular interaction is high and the molecules do not move easily. Accordingly, they cannot follow the upper wall movement, and a small slips occurs. Since the nonlinear responses increase with increasing pressure, the slips seem to occur between the walls and the film. Nonlinear responses represent the surface energy roughness of the upper wall. Further, since the slider movement is slower at lower frequencies, the film molecules move along the surface (that is, move through energy minimum points) and nonlinear responses increase.

Figure 12 shows the frequency dependence of viscosity. The viscosity decreases with increasing frequency; that is, shear thinning is observed. As a comparison, Figure 13 shows the frequency dependence of viscosity of low-density systems used in Figure 3 in section 3.2. It is not so clear, but shear thinning seems to begin at lower frequency with higher pressure in Figure 13. This frequency corresponds to the critical frequency ω_c as mentioned in section 3.2, and this is consistent with Rouse theory.[18] In experiments, the slope of the logarithm of viscosity versus the logarithm of frequency was between −2/3 and −1 and shear shinning begins at a certain shear rate (frequency).[3] In computer simulations, shear thinning has also been observed[9,11] and it was also observed that the critical shear rate, at which shear thinning begins, was slower with higher pressure.[29] In our simulations, the slope increases with higher pressure. The minimum slope is about −1/2 and the maximum one is about −1. Shear thinning can be considered theoretically. Subbotin et al.[30] predicted that shear thinning was caused by elongation of molecules. However, since shear thinning occurs even in the linear response region, elongation of molecules is not the cause of the shear thinning at least in the present work. Further, the tendency for shear thinning is stronger with increasing pressure, in other words, with the

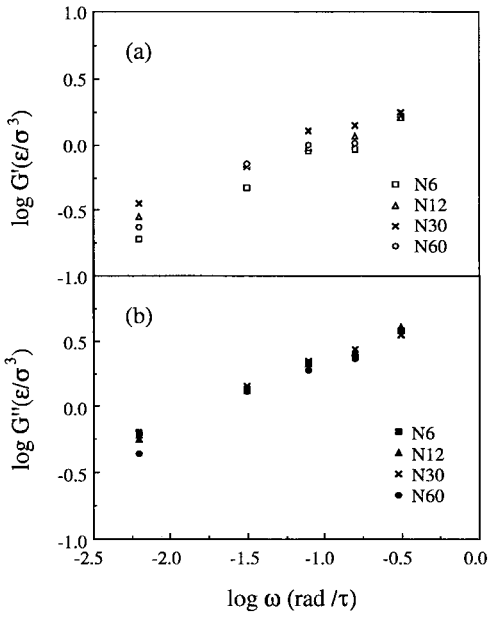

Figure 14. Comparison of the frequency dependence of (a) storage and (b) loss moduli for different molecular lengths with film thickness of about 6.8σ.

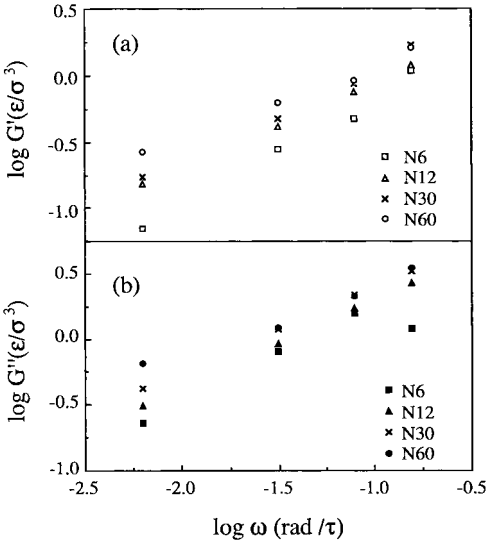

Figure 15. Comparison of the frequency dependence of (a) storage and (b) loss moduli for different molecular lengths with a film thickness of about 12.8σ.

decreasing of G''/G'. This indicates that the glassy-like condition causes the increase of shear thinning.

3.6. Influence of Molecular Chain Length. Figure 14 shows the frequency dependence of storage and loss moduli with a film thickness of about 6.8σ and Figure 15 shows it for a film thickness of about 12.8σ confined by repulsive walls. Figure 14a,b indicates that there is almost no molecular length dependence for the storage and loss moduli in the thin film. But in Figure 15a,b, storage and loss moduli increase with longer molecular length in the thick film. This tendency has also been observed in an experiment with a confined film.[13] Table 2 shows that there are almost no differences for R_g and anisotropy of R_g between thin and thick film. According to the Rouse theory as shown in eqs 21 and 22, the storage and loss moduli should increase with increasing molecular weight, since relaxation time is longer with higher molecular weight. The increase of storage and loss moduli with longer molecular chain length has also been observed in an experiment with the bulk state.[18] We suppose that if the influence of the wall is strong, the longest relaxation time difference between different molecular chain lengths would become small, so the storage and loss moduli would become almost the same, independent of molecular chain length in thin film. Unfortunately, the relaxation time of the thin film was so long that we could not measure them. These results indicate that when the film is thin enough, the frictional coefficient between walls and film is almost independent of molecular weight under the ideal condition.

For the film thickness of 4.5σ, the phase of the shear stress of the upper wall and that of the base is considerably different at least when the logarithm of the frequency is larger than −2.3, because the velocity gradient of the film is not uniform for a thinner film than 4.5σ. Also, when the logarithm of the frequency is larger than about 0.0 in other films, their film velocity gradient is not uniform and we cannot measure the storage and shear moduli for films thinner than 6.8σ with repulsive walls.

4. Conclusions

We have investigated the storage and loss moduli of a confined thin film by using molecular dynamics simulations of the bead-spring model. The simulation results showed that even if the film was thinner than 5 molecular diameters, the frequency dependence of storage and loss moduli was consistent with that of Rouse theory. The critical frequency at which storage and loss moduli begin to be proportional to the square of the frequency was found to be higher with higher densities. Further, the Rouse time, derived from the relaxation time of end-to-end vector correlation function, in regions close to the wall was longer than that inside the film. The critical frequency was found to be dominated by Rouse time inside the film rather than by the averaged Rouse time of the whole molecule. At high pressures, storage and loss moduli were almost independent of frequency and this indicated the film was solidlike. Shear thinning was observed at values higher than the critical frequency and this effect became larger with the solidlike film. Such shear thinning has been observed in SFA experiments. Hardly any molecular chain length dependence of the storage and loss moduli was observed in the thin film in the high-frequency region, since the longest relaxation time difference between different molecular chain lengths became negligible because of the greater influence of wall−film interactions.

The frequency dependence of storage and loss moduli derived from the Green−Kubo formula was roughly similar to that calculated from the shear response by a slider sheared periodically, but absolute values of the Green−Kubo formula were much smaller than those of the other method. These differences were explained as follows. Since the Green−Kubo formula uses fluctuations of the pressure tensor, if the number of the atoms making up the film is not large and the simulation time is not long enough, values of storage and loss moduli are unstable. Further, even at small amplitude, the shear response contains some nonlinear response. Since the amplitude is larger than that in the region of linear shear response, the storage and loss moduli calculated from shear response would become larger than those by the Green−Kubo formula. However, more work is necessary to elucidate the difference clearly.

Acknowledgment. We are grateful for helpful discussions with Dr. M. Yoneya and Mr. Y. Ito of Hitachi Research Laboratory.

References and Notes

(1) Israelachvili, J. N.; McGuiggan, P. M.; Homola, A. M. *Science* **1988**, *61*, 2570.
(2) Gee, M. L.; MacGuiggan P. N.; Israelachvili, J. M.; Homola, A. M. *J. Chem. Phys.* **1990**, *93*, 1895.
(3) Granick, S. *Science* **1991**, *253*, 1374.
(4) Riter, G.; Demirel, A. L.; Granick, S. *Science* **1994**, *263*, 1741.
(5) Demirel, A. L.; Granick, S. *Phys. Rev. Lett.* **1996**, *77*, 4330.
(6) For review of FFM, see: Overney, R. M.; Meyer, E. *MRS Bull.* **1993**, May, 26.
(7) Thompson, P. A.; Grest, G. S.; Robbins, M. O. *Phys. Rev. Lett.* **1992**, *68*, 3448.
(8) Manias, E.; Hadziioannou, G.; Bitsanis, I.; ten Brinke, G. *Europhys. Lett.* **1993**, *24*, 99.
(9) Reiter, G.; Demirel, A. L.; Peanasky, J.; Cai, L. L.; Granick, S. *J. Chem. Phys.* **1994**, *101*, 2606.
(10) Stevens, M. J.; Mondello, M.; Grest, G. S.; Cui, S. T.; Cochran, H. D.; Cummings, P. T. *J. Chem. Phys.* **1997**, *106*, 7303.
(11) Tanaka, K.; Takahara, A.; Kajiyama, T. *Macromolecules* **1996**, *29*, 4050.
(12) Kajiyama, T.; Tanaka, K.; Takahara, A. *Macromolecules* **1997**, *30*, 280.
(13) Granick, S.; Hu, H.-W. *Langmuir* **1994**, *10*, 3857.
(14) Granick, S.; Hu, H.-W.; Carson, G. A. *Langmuir* **1994**, *10*, 3867.
(15) Peanasky, J.; Cai, L. L.; Granick, S.; Kassel, C. R. *Langmuir* **1994**, *10*, 3874.
(16) Felderhof, B. U.; Deutch, J. M.; Titulaer, U. M. *J. Chem. Phys.* **1975**, *63*, 740.
(17) Diaz, F. G.; de la Torre, J. G. *J. Chem. Phys.* **1994**, *27*, 5371.
(18) Ferry, J. D. *Viscoelastic Properties of Polymers*; Wiley: New York, 1980.
(19) Evans, D. J.; Morris, G. P. *Stastical Mechanics of Nonequilibrium Liquids*; Academic Press: London, 1990.
(20) Mondello, M.; Grest, G. S. *J. Chem. Phys.* **1997**, *106*, 9327.
(21) Grest, G. S.; Kremer, K. *Phys. Rev. A* **1986**, *33*, 3628.
(22) Thompson, P. A; Robins, M. O. *Phys. Rev. A* **1990**, *41*, 6380.
(23) Berendsen, H. J. C.; Postma, J. P. M.; van Gunsteren, W. F.; DiNola, A.; Haak, J. R. *J. Chem. Phys.* **1984**, *81*, 3684.
(24) Hockney, R. W. *Methods Comput. Phys.* **1976**, *20*, 136.
(25) Matsumoto, T.; Segawa, Y.; Warashina, Y.; Onogi, S. *Trans. Soc. Rheol.* **1973**, *17*, 47.
(26) Doi, M.; Edwards, S. F. *The Theory of Polymer Dynamics*; Oxford University Press: New York, 1986.
(27) Bitsanis, I.; Hadziioannou, G. *J. Chem. Phys.* **1990**, *92*, 3827.
(28) Kremer, K.; Grest, G. S. *J. Chem. Phys.* **1990**, *92*, 5057.
(29) Thompson, P. A.; Robbins, M. O.; Grest, G. S. *Israel J. Chem.* **1995**, *35*, 93.
(30) Subbotin, A.; Semenov, A.; Hadziioannou, G.; ten Brinke, G. *Macromolecules* **1993**, *28*, 3898.

MA971343T